New insights into the differences between the dual node approach and the common node approach for coupling surface-subsurface flow

Rob de Rooij

Water Institute, University of Florida, 570 Weil Hall, PO Box 116601, Gainesville, FL-32611-6601, USA

r.derooij@ufl.edu

Corresponding author:

Rob de Rooij

Water Institute

University of Florida

570 Weil Hall

PO Box 116601

Gainesville

FL-32611-6601

USA

Telephone: 1-352-392-5893

Fax: 1-352-392-6855

Key points

Surface-subsurface flow coupling

Abstract

The common node approach and the dual node approach are two widely applied approaches to couple surface-subsurface flow. In this study both approaches are analyzed for cell-centered as well as vertex-centered finite difference schemes. It is shown that the dual node approach should be conceptualized and implemented as a one-sided first-order finite-difference to approximate the vertical subsurface hydraulic gradient at the land surface. This results in a consistent dual node approach in which the coupling length is related to grid topology. In this coupling approach the coupling length is not to be interpreted as a non-physical model parameter. Although, this particular coupling approach is technically not new, the differences between this consistent dual node approach and the common node approach have not been studied in detail. In fact, this coupling scheme is often believed to be similar to the common node approach. In this study it is illustrated that in comparison to the common node approach, the head continuity at the surface-subsurface interface is formulated more correctly in the consistent dual node approach. Numerical experiments indicate that the consistent dual node approach is less sensitive to the vertical discretization when simulating excess infiltration. It is also found that the consistent dual node approach can be advantageous in terms of numerical efficiency.

1 Introduction

There exists a variety of hydrogeological problems, such as the hydrologic response of hillslopes and river catchments, which requires an integrated analysis of surface and subsurface flows. This has led to the development of physically-based, distributed parameter models for simulating coupled surface-subsurface flows. Well-known examples of such models include MODHMS [*Kollet and Maxwell*, 2006; *Panday and Huyakorn*, 2004] , InHM [*Ebel et al.*, 2009], HydroGeoSphere [*Therrien et al.*, 2010], CATHY [*Camporese et al.*, 2010], WASH123D [*Yeh et al.*, 2011], ParFlow [*Kollet and Maxwell*, 2006] and OpenGeoSys [*Kolditz and Shao*, 2010]. Typically, subsurface flow is governed by the Richards' equation whereas surface flow is either governed by the kinematic wave or the diffusive wave equation.

The coupling between subsurface and surface flow may be either based on the common node approach [*Kollet and Maxwell*, 2006] or on the dual node approach [*Ebel et al.*, 2009; *Panday and Huyakorn*, 2004; *VanderKwaak*, 1999]. In the common node approach coupling is formulated by a continuity in head between surface and subsurface nodes. The dual node approach is based on formulating an exchange flux between the surface and subsurface nodes. Typically, the dual node approach is conceptualized as a hydraulic separation of the surface and the subsurface by an interface with a given thickness [*Liggett et al.*, 2012]. The thickness of this interface defines a coupling length between the dual nodes to formulate the discrete exchange flux between the dual nodes.

It has been argued that the coupling length represents a non-physical model parameter, because there is often no evidence to support the existence of a distinct interface between the two flow domains [*Kollet and Maxwell*, 2006]. As such it appears that the common node approach is a more physically based coupling approach [*Kollet and Maxwell*, 2006; *Liggett et al.*, 2012]. It has

86 also been found that accurate simulations based on the dual node approach typically require a very
87 small coupling length [*Ebel et al.*, 2009; *Liggett et al.*, 2012; *Liggett et al.*, 2013]. Since it is known
88 that the dual node approach mimics the common node in the limit as the coupling length goes to
89 zero [*Ebel et al.*, 2009], it thus seems that the dual node approach is most accurate if it mimics the
90 common node approach. Nonetheless, it has been argued that the dual node approach remains an
91 attractive alternative coupling approach since it offers more flexibility than the common node
92 approach. Namely, while it can mimic the common node approach, the dual node approach offers
93 the possibility to simulate a less tight coupling of surface-subsurface flow which results in
94 increased computational efficiency [*Ebel et al.*, 2009].

95 In this study a detailed analysis of both coupling approaches is provided for cell-centered
96 as well as vertex-centered finite difference schemes. This analysis starts with the crucial
97 observation that that the topmost subsurface nodal values as computed by the finite difference
98 schemes represent the mean values within the topmost discrete control volumes. Numerical
99 experiments to compare the coupling approaches are carried out with the model code DisCo [*de*
100 *Rooij et al.*, 2013]. It is shown that the dual node approach should be interpreted and implemented
101 as a one-sided finite difference approximation of the vertical hydraulic gradient at the land surface.
102 This yields a consistent dual node scheme in which the coupling length is defined by the half the
103 thickness of the topmost subsurface cells. The scheme of An and Yu [*An and Yu*, 2014] as well as
104 the scheme of Kumar et al. [*Kumar et al.*, 2009] are essentially very similar to this consistent dual
105 node scheme. In the work of Panday and Huyakorn [*Panday and Huyakorn*, 2004], one of the
106 suggestions to define the coupling length is to use half the thickness of the topmost subsurface
107 cells, which yields a consistent dual node scheme. While the idea that the coupling length can be
108 based on the grid topology is not new [*Panday and Huyakorn*, 2004], the idea that it must be

related to grid topology to obtain a consistent approach is a significant new insight. Namely, since the coupling length in the consistent dual node approach is not to be interpreted as the thickness of a layer that separates the subsurface from the surface, the consistent dual node approach is not automatically less physically based than the common node. In fact, as explained in this study in comparison to the common node approach the implementation of a head continuity at the surface-subsurface interface is formulated more correctly in the consistent dual node approach.

The current consensus about how the dual node approach compares to the common node approach is based on alternative dual node approaches which as explained in this study are different from the consistent dual node approach. In this study the consistent dual node approach is compared in detail with the common node approach. It is shown that if the vertical discretization is sufficiently fine, then the common node approach and the consistent dual node approach are equally accurate. However, when simulating excess infiltration the consistent dual node approach is found to be less sensitive to the vertical discretization in comparison to the common node approach. This advantage in accuracy is related to the fact that head continuity is more correctly formulated in the consistent dual node approach. Moreover, it is also shown that the consistent dual node approach can be advantages in terms of numerical efficiency when simulating runoff due to both excess saturation as well as excess infiltration. The finding of this study show that the consistent dual node approach compares more positively with respect to the common node approach than other dual node approaches.

2 Interpretation of nodal values

As explained later on, a correct interpretation of nodal values is crucial for understanding the dual and common node approach for coupling surface-subsurface flow. Moreover, both coupling

approaches depend on the configuration of surface and topmost subsurface nodes near the land surface. This configuration depends on whether cell-centered or vertex-centered schemes are used. In this study both type of schemes will be covered, but for simplicity only finite difference schemes are considered.

In both cell-centered as vertex-centered schemes the flow variables such as the heads and the saturation are computed on nodes. In vertex-centered schemes these nodes coincide with the vertices of mesh, whereas in cell-centered schemes the nodes coincide with the cell centers. When employing a finite difference scheme, nodal values correspond to the mean value within surrounding discrete control volumes. In cell-centered finite difference schemes these discrete volumes are defined by the primary grid cells. In vertex-centered finite difference schemes these discrete volumes are defined by the dual grid cells. Ideally, the mean values in the discrete control volumes are derived by applying the midpoint rule for numerical integration such that their approximation is second-order accurate. Therefore, the nodal values should ideally represent values at the centroid of the surrounding discrete control volume [*Blazek*, 2005; *Moukalled et al.*, 2016]. In that regard, a cell-centered finite difference scheme is thus more accurate than a vertex-centered finite difference scheme. Namely, in cell-centered finite difference schemes the nodal values always correspond to the centroids of the cell whereas in vertex-centered finite difference schemes nodes and centroids (of the dual cells) do not coincide at model boundaries and in model regions where the primary grid is not uniform. It is well-known that this mismatch between nodes and centroids can lead to inaccuracies since the mean values within affected discrete volumes are not computed by a midpoint rule [*Blazek*, 2005; *Moukalled et al.*, 2016].

Typically, vertex-centered schemes for simulating coupled surface-subsurface flow are based on mass-lumped finite element schemes [*Liggett et al.*, 2012]and not on finite difference

schemes. However, with respect to coupling surface-subsurface flow there is actually no difference between a mass-lumped finite element scheme and a vertex-centered finite difference scheme. Similar as in vertex-centered finite difference schemes, the nodal values in mass-lumped finite element schemes define the mean values inside dual grid cells [*Zienkiewicz et al.*, 2005]. Moreover, the coupling approaches establish one-to-one relations between surface and topmost subsurface nodes which do not depend on whether a finite difference or a finite element approach is being used.

3 Common node approach

The common node approach defines a head continuity between the topmost subsurface nodes and the surface nodes. This continuity requires that the topmost subsurface nodes and the surface nodes are co-located at the land surface such that there exists a continuity in the elevation head. This requirement is automatically full-filled in vertex-centered schemes. Figure 1a illustrates the configuration of common nodes in ParFlow, a cell-centered scheme [personal communication Maxwell, R. in relation to previous work of the author [*De Rooij et al.*, 2012]]. Figure 1c illustrates the configuration of common nodes for vertex-centered schemes. This configuration is similar to the configuration as used in HydroGeoSphere [*Therrien et al.*, 2010].

Considering that nodal values represent ideally the mean values within discrete control volumes as described in Section 2, it can be argued that the head continuity as implemented in the common node approach is not in agreement with the physical principle of head continuity at the land surface. Namely, the common node approach enforces a continuity between surface heads at the land surface and the mean subsurface heads within the topmost subsurface discrete control volumes which have a finite thickness. This is different from enforcing a continuity between

surface heads and subsurface heads within an infinitesimal thin subsurface layer directly below the land surface. As such the common node approach is only numerically correct if the topmost subsurface cells are very thin.

4 Dual node approach

4.1 Basics

Figure 1b and 1c illustrate the classical arrangement of surface and subsurface nodes in cell-centered and vertex-centered finite difference schemes, respectively. Commonly, the dual node approach is expressed in terms of an exchange flux q_e [LT^{-1}] computed as [*Liggett et al.*, 2012; *Panday and Huyakorn*, 2004]:

$$q_e = f_p \frac{K_z}{l}\left(h_s - h_{ss}\right) \tag{1}$$

where h_s and h_{ss} are the hydraulic heads [L] associated with the surface node and the topmost subsurface node, respectively, f_p [-] the fraction of the interface that is ponded and l the coupling length [L]. The ponded fraction of the interface is typically defined by a function that varies smoothly between zero at the land surface elevation and unity at the rill storage height which defines the minimum water depth for initiating lateral overland flow [*Panday and Huyakorn*, 2004]. In equation (1) the term $f_p K_z / l$ is commonly referred to as the first-order exchange parameter, where first-order means that the exchange flux depends linearly of the hydraulic head difference.

Typically, equation (1) is not derived as a numerical approximation of basic flow equations that govern the exchange flux, but is merely presented a numerical technique to couple two different flow domains [*Ebel et al.*, 2009; *Liggett et al.*, 2012]. Subsequently, the dual node

approach is conceptualized by interpreting equation (1) as an expression that describes groundwater flow across a distinct interface separating the two flow domains [*Ebel et al.*, 2009; *Liggett et al.*, 2012; *Liggett et al.*, 2013].

4.2 Consistent dual node approach

In the following, it is illustrated that the dual node approach can and should be derived from basic equations that describe infiltration into a porous medium. Using Darcy's Law, the infiltration rate at the ponded land surface $q_{s\to ss}$ [LT^{-1}] can be written as a function of the vertical subsurface hydraulic gradient at the land surface:

$$q_{s\to ss} = \left(k_r K_z \frac{\partial h}{\partial z} \right)\Bigg|_{z=z_s} = K_z \frac{\partial h}{\partial z}\Bigg|_{z=z_s} \tag{2}$$

where h the hydraulic head [L], z the elevation head [L], k_r the relative hydraulic conductivity [-] K_z the saturated vertical hydraulic conductivity [LT^{-1}] and z_s the elevation head at the land surface. The relative hydraulic conductivity is unity because equation (2) applies to the ponded land surface which implies fully saturated conditions at the land surface (i.e. ponding means $p_s > 0$, where p_s is the pressure head at the surface). Similarly, the infiltrability [LT^{-1}], defined as the infiltration rate under the condition of atmospheric pressure [*Hillel*, 1982], can be written as:

$$I = \left(k_r K_z \frac{\partial h}{\partial z} \right)\Bigg|_{z=z_s,\, p_s=0} = K_z \frac{\partial h}{\partial z}\Bigg|_{z=z_s} \tag{3}$$

The relative hydraulic conductivity is again unity because the saturation equals unity under atmospheric conditions ($p_s = 0$). The infiltration rate at non-ponded land surface $q_{atm\to ss}$ [LT^{-1}] can be expressed as:

$$q_{atm\to ss} = \min\left(\max\left(I, 0 \right), q_R \right) \tag{4}$$

where q_R is the effective rainfall rate (i.e. the infiltration rate is limited by either the infiltrability or the available effective rainfall rate). The total exchange flux across the surface-subsurface interface can now be written as:

$$q_e = f_p q_{s\to ss} + \left(1 - f_p\right) q_{atm\to ss} \tag{5}$$

To approximate the vertical subsurface hydraulic gradient in equations (2) and (3) , it is crucial to recognize that according to the principle of head continuity at the land surface, the surface hydraulic head at a surface node must also represent the subsurface head at the land surface at that location. Moreover, since the subsurface hydraulic heads at the topmost subsurface nodes are ideally associated with the centroids of the topmost subsurface discrete control volumes, these head values do not represent values at the land surface but at some depth below the land surface. Because the subsurface hydraulic heads at the dual nodes can be and should be associated with a different elevation, the vertical subsurface head gradient between the dual nodes can be approximated by a standard finite difference approximation. If this approximation is being used to approximate the gradient at the land surface in equations (2) and (3), then this approximation is by definition a one-sided first-order finite difference. Defining the coupling length by $l = \Delta z_{dn}$ where Δz_{dn} is the difference in the mean elevation head associated with the dual nodes, the infiltration rate and infiltrability can thus be computed with the following one-sided finite difference approximation:

$$K_z \left.\frac{\partial h}{\partial z}\right|_{z=z_s} \approx \frac{K_z}{l}\left(h_s - h_{ss}\right) \tag{6}$$

The above definition of the coupling length $l = \Delta z_{dn}$ ensures a proper approximation of the vertical gradient in elevation head at the land surface:

238 $$\left.\frac{\partial z}{\partial z}\right|_{z=z_s} = \frac{\Delta z_{dn}}{l} = 1 \quad (7)$$

239 The above derivation of the consistent dual node approach from basic flow equations has
240 implications for how the dual node approach is conceptualized and how it should be implemented.
241 The idea that the coupling length must be directly related to the spatial discretization is an
242 important new insight. Namely, as the coupling length is related to grid topology, it does not
243 represent a non-physical parameter associated with a distinct interface separating the two domains.
244 It is also crucial to observe the difference between the consistent dual node approach and the
245 common node approach regarding how the head continuity at the surface-subsurface interface is
246 formulated. As explained in Section 2, the formulation in the common node approach is only
247 correct if the topmost subsurface discrete volumes are very thin. In comparison, the formulation
248 in the dual node approach is correct irrespective of the vertical discretization. Namely, irrespective
249 of the vertical discretization the surface hydraulic heads equal the subsurface heads at the interface.

250 Since nodal values in cell-centered scheme are located at the centroids of the cells, the
251 coupling length is simply given by $l = z_s - z_{ss}$ where z_s and z_{ss} are the elevation heads [L] associated
252 with the surface node and the topmost subsurface node, respectively. This value for the coupling
253 length in cell-centered schemes has also been suggested by Panday and Huyakorn [*Panday and*
254 *Huyakorn*, 2004]. However, in their work, the particular advantage of choosing this value (i.e.
255 maintaining a unit gradient in elevation head) is not recognized. The coupling schemes as used by
256 An and Yu [*An and Yu*, 2014] and Kumar et al. [*Kumar et al.*, 2009] are also in essence consistent
257 dual node schemes. However, these schemes are not recognized as a dual node scheme. Instead,
258 An and Yu [*An and Yu*, 2014] argue that their scheme is similar to the common node approach of
259 Kollet and Maxwell [*Kollet and Maxwell*, 2006]. Kumar et al. [*Kumar et al.*, 2009] argue that their

scheme is similar to the dual node approach if the coupling length goes to zero which implies that their scheme would be similar to the common node approach. However, contrary to the common node approach the schemes of An and Yu [*An and Yu*, 2014] and Kumar et al. [*Kumar et al.*, 2009] compute exchange fluxes between surface and topmost subsurface nodes and therefore these schemes are technically dual node schemes. As explained in this study, it is crucial to observe that the schemes of An and Yu [*An and Yu*, 2014] and Kumar et al. [*Kumar et al.*, 2009] are actually quite different from the common node approach. As already mentioned, the consistent dual node scheme differs from the common node approach with respect to how the head continuity is formulated at the surface-subsurface interface. As discussed later on, this difference has crucial consequences in terms of accuracy as well as numerical efficiency.

In vertex-centered schemes the commonly used nodal configuration near the surface is such that $z_s = z_{ss}$. However, even though the topmost subsurface node is located at the land surface in a vertex-centered scheme, the elevation head at this node should ideally correspond to the mean elevation head within the topmost subsurface discrete volume. This suggests that the topmost subsurface node should be moved to the centroid of the topmost subsurface discrete volume. Although this is a possible solution, the drawback of this solution is that the subsurface model ceases to be a purely vertex-centered scheme. Moreover, such an operation cannot be performed in finite element schemes since the nodal positions define the geometry of the elements. Therefore, an alternative solution is proposed. Namely, in vertex-centered schemes the elevation of the surface nodes are changed according to $z_s = z_{ss} + l$ where l is equals half the thickness of the topmost subsurface dual cell. The resulting nodal configuration is illustrated in Figure 1d. When applying this solution, all the topmost subsurface cells must have the same thickness, such that the topography is increased with the same value everywhere. In essence, the motivation behind this

283 solution is that a more accurate approximation the hydraulic gradient (i.e. enforcing a unit gradient
284 in elevation head) is more important than the actual elevation of the land surface. Similar to the
285 nodal configuration in ParFlow, the resulting nodal configuration may not seem ideal. Namely, the
286 surface elevation does not coincide with the top of the subsurface grid. Nonetheless, as illustrated
287 later on, simulation results obtained with the resulting scheme are reasonable.

288 To illustrate that the presented dual node approach exhibits consistent behaviour, the
289 necessary conditions for ponding due to excess infiltration and exfiltration are considered. In
290 general ponding starts when $q_R > I$ [*Hillel*, 1982]. Setting $q_R = I$, $p_s = 0$ and using $h = p + z$, it
291 follows from equation (6) and (7) that at the moment of ponding:

292 $$p_{ss} = l\left(1 - \frac{q_R}{K_z}\right) \tag{8}$$

293 Ponding due to excess infiltration occurs if $q_R / K_z > 1$ and implies that saturation in the subsurface
294 starts from the top down [*Hillel*, 1982]. Using $q_R / K_z > 1$ it follows from equation (8) that ponding
295 due to excess infiltration occurs while $p_{ss} < 0$. This is reasonable since this value represents the
296 pressure head at a certain depth below the land surface. Namely, if saturation occurs from the top-
297 down then the saturation at a certain depth occurs later than saturation at the land surface. It is
298 noted that if the ratio q_R / K_z is greater than but close to unity or if the coupling length is very small,
299 then this condition becomes $p_{ss} \approx 0$. Once ponding starts the total flux rate between the dual nodes
300 equals $K_z\left(\left(p_s - p_{ss}\right)/l + 1\right)$. Top-down saturation requires that this flux exceeds the vertical
301 hydraulic conductivity. Reaching saturation at the topmost node ($p_{ss} = 0$) therefore requires $p_s \geq 0$
302 . Thus, top-down saturation will occur after ponding is initiated. Ponding due to excess saturation
303 occurs if $q_R / K_z < 1$ and implies that saturation in the subsurface starts from the bottom up [*Hillel*,

1982]. It follows from equation (8) that ponding due to excess saturation occurs while $0 < p_{ss} < l$. Thus ponding starts after reaching fully saturated conditions at the topmost subsurface node, which is again reasonable. It is noted that if the ratio q_R / K_z is smaller than but close to unity or if the coupling length is very small, then ponding occurs when $p_{ss} \approx 0$.

4.3 Comparison to alternative coupling approaches

To illustrate that it is crucial to account for the meaning of the values at the topmost subsurface nodes, it is instructive to consider what happens if these values are not taken as the mean values within discrete control volumes. As a first example, consider vertex-centered schemes where the dual nodes are defined such that $z_{ss} = z_s$ as illustrated in Figure 1c. This is inconsistent because it defines a zero gradient in elevation head between the dual nodes. Since the vertical gradient in elevation head between the dual nodes is zero the total flux rate after ponding now equals $K_z (p_s - p_{ss})/l$. Top-down saturation requires that this flux exceeds the vertical hydraulic conductivity. Thus, reaching saturation at the topmost subsurface node ($p_{ss} = 0$) requires $p_s > l$. Therefore, top-down saturation will not occur if runoff occurs and if the surface water depths remains smaller than the chosen coupling length. Indeed, it has been pointed out in other studies that the coupling length should be smaller than the rill storage height [*Delfs et al.*, 2009; *Liggett et al.*, 2012]. The zero vertical gradient in elevation head between the dual nodal also means that the required condition for ponding now becomes $p_{ss} = -l q_R / K_z$. This implies that ponding due to excess saturation occurs while the topmost subsurface node is not yet saturated. This dual node approach has been compared to the common node approach in vertex-centered schemes [*Liggett et al.*, 2012].

A second example is the dual node approach for cell-centered schemes as implemented in MODHMS which uses an adapted pressure-saturation relationship for the topmost subsurface nodes such that the topmost subsurface node only becomes fully saturated if hydraulic head at the node rises above the land surface [*Liggett et al.*, 2013]. Since the topmost subsurface heads are associated with the cell centroid, this dual node scheme defines a unit gradient in elevation head at the land surface. However, the saturation value at the topmost node is associated with a location at the land surface and not with the centroid of a discrete control volume. This has undesirable consequences. Namely, saturating the topmost subsurface node ($p_{ss} = l$) due to excess infiltration requires that $p_s > l$. Indeed, when simulating excess infiltration with MODHMS, a very small coupling length is needed to simulate top-down saturation due to excess infiltration. [*Gaukroger and Werner*, 2011; *Liggett et al.*, 2013]. It can also be shown that ponding due to excess saturation occurs while $0 < p_{ss} < l$. But, because of the adapted pressure-saturation relationship this means that ponding starts while the topmost subsurface node is not yet saturated. This dual node approach has been compared to the common node approach in cell-centered schemes [*Liggett et al.*, 2013].

The two comparison studies of Liggett et al. [*Liggett et al.*, 2012; *Liggett et al.*, 2013] indicate that the dual node approach is typically only competitive with the common node approach in terms of accuracy once the coupling length is very small. However, the requirement for a very small coupling length, is a logical consequence if the topmost subsurface nodal values are not taken as the mean values within discrete volumes. In essence, by choosing a very small coupling length this inconsistency is minimized. This contrasts with the consistent dual approach in which decreasing the coupling length for a given vertical discretization will result in more inaccurate simulation results as this would be numerically incorrect.

CATHY [*Camporese et al.*, 2010] as well as the model of Morita and Yen [*Morita and Yen*, 2002] are examples of models which are neither based on the common node approach, nor a dual node approach. Both these models are conjunctive models in which the surface and subsurface flow are computed separately in a sequential fashion and in which coupling is established by matching the flow conditions along the surface-subsurface interface. A complete discussion is outside the scope of this paper, but it is worthwhile to mention that these models share some crucial characteristics with the consistent dual node approach. Although the two models are different, both models switch between appropriate boundary conditions along the surface-subsurface interface, such that infiltration fluxes are limited to the infiltrability. In both models the infiltration fluxes are computed while accounting for the unit vertical gradient in elevation head near the surface-subsurface interface. In addition, in both models ponding occurs when the infiltrability is exceeded.

5 Numerical experiments

5.1 Numerical model

To compare the consistent dual node approach with respect to the common node approach in terms of accuracy and computational efficiency numerical experiments are presented. These experiments are carried out with the model code DisCo. This model code can simulate coupled surface-subsurface flow with the dual node approach using a fully implicit or monolithic scheme [*de Rooij et al.*, 2013]. Subsurface flow is governed by the Richards' equation while surface flow is governed by the diffusive wave equation.

Starting from a dual node scheme, the implementation of a common node scheme is relatively straightforward. If the surface nodes are numbered last, a permutation vector can be

constructed which gives the corresponding topmost subsurface node for each surface node. Then, the node numbering as used in the original dual node scheme can still be used to compute the surface and subsurface flow terms. Subsequently, using the permutation vector the surface and subsurface flow terms associated with a common node can be combined into the same row of the global matrix system. In addition, when using the common node approach, there is no need to evaluate exchange flow terms between the two flow domains. It is noted that the surface flow and subsurface flow computations are exactly the same irrespective of the coupling approach. As such the model permits to compare the two approaches in terms of accuracy as well as numerical efficiency.

An adaptive error-controlled predictor-corrector one-step Newton scheme [*Diersch and Perrochet*, 1999] is used in which a single user-specified parameter controls the convergence as well the time stepping regime. Although, this scheme may not be necessary the most efficient scheme, it ensures that time discretization error is the same irrespective of the applied coupling approach. For brevity further details about the model are not discussed here and can be found elsewhere [*de Rooij et al.*, 2013].

5.2 Hillslope scenarios

The model code is applied to a set of three hillslope scenarios. Table 1 lists the abbreviations used in the figures to distinguish between the coupling approaches, and to distinguish between cell-centered and vertex-centered schemes. Each scenarios is solved using different but uniform vertical discretizations and Δz specifies the discretization of the primary grid. The first two simulation scenarios consider hillslope problems as designed by Sulis et al. [*Sulis et al.*, 2010]. For the purpose of this study, a third scenario is considered in which the initial and boundary conditions are different to create a flooding wave across an unsaturated hillslope. The problems

392 consist of a land surface with a slope of 0.05 which is underlain by a porous medium. The domain
393 is 400 m long and 80 m wide. The subsurface is 5 m thick. In the direction of the length and in the
394 direction of the width the discretization is 80 m. Different vertical discretizations are considered.
395 The van Genuchten parameters are given by $s_r = 0.2$, $s_s = 1.0$, $\alpha = 1$ m^{-1} and $n = 2$. The porosity is
396 0.4 and the specific storage is 10^{-4} m^{-1}. The manning's roughness coefficients are given by 3.3 x
397 10^{-4} m$^{-1/3}$min. The surface flow domain has a zero-gradient outflow condition. For the first two
398 simulation scenarios the domain is recharged with an effective rainfall rate of 3.3 x 10^{-4} m/min for
399 a duration of 200 minutes and the initial water table depth is at a depth of 1.0 m below the land
400 surface.

401 The first scenario considers excess saturation, the saturated conductivity equals 6.94 x 10^{-}
402 ^{4} m/min. Figure 2 and 3 illustrates the simulated runoff and the number of Newton steps,
403 respectively. Figure 4 and 5 illustrate the subsurface pressure heads at the topmost subsurface
404 nodes and the water depths on the surface nodes. For the second scenario which considers excess
405 infiltration the saturated hydraulic conductivity equals 6.94 x 10^{-7} m/min. Figure 6 and 7 show the
406 simulated runoff and the number of Newton steps, respectively. Figure 8 and 9 illustrate the
407 subsurface pressure heads at the topmost subsurface nodes and the water depths on the surface
408 nodes for the finest and the coarsest vertical discretization, respectively. In the third scenario a
409 surface water flood wave crossing the hillslope in the downhill direction is simulated by applying
410 a Neumann boundary condition of 1.0 m^3/s for a duration of 200 minutes to the surface nodes with
411 the highest elevation. The initial water table is located at a depth of 1.5 m. The vertical saturated
412 hydraulic conductivity equals 6.94 x 10^{-6} m/min. Figure 10 illustrates the differences in simulated
413 runoff and Figure 11 illustrates the number of Newton steps of the model runs. Figure 12 and 13

illustrate the subsurface pressure heads at the topmost subsurface nodes and the water depths on the surface nodes for the finest and the coarsest vertical discretization, respectively.

6 Discussion

6.1 Accuracy

As discussed by Ebel et al. [*Ebel et al.*, 2009] and confirmed by others [*Liggett et al.*, 2012] the dual node approach mimics the common node approach if the coupling length becomes sufficiently small. When comparing the consistent dual node approach and the common node approach a very similar observation applies. If the topmost subsurface cells are very thin, then the coupling length in the consistent dual node approach is very small. Also, if the topmost subsurface cells are sufficiently thin then the formulation of head continuity at the surface-subsurface interface in the common node approach is correct. Thus, the common node approach will mimic the consistent dual node approach. Indeed, the simulations results indicate that a relatively fine vertical discretization yields similar results for the common node approach as well as for the consistent dual node approach (Figure 2a, 4a, 6a, 8a, 10a and 12a).

A relatively fine uniform vertical discretisation also enables to simulate sharp saturation fronts with the Richards' equation [*Pan and Wierenga*, 1995; *Ross*, 1990]. As such the simulation results based on the finest vertical discretization can be taken as reference solutions that enables comparisons of the coupling approaches when a coarser vertical discretization is used.

6.1.1 Excess saturation

The simulation results of runoff due to excess saturation as obtained by the common node approach and the consistent dual node approach as depicted in Figure 2 illustrate that simulating excess saturation runoff is not significantly affected by the vertical discretization. This is because the time

436 needed to reach fully saturated conditions in the subsurface is a simple function of the flow
437 boundary conditions and the initial water content. It is thus expected that the vertical discretization
438 does not significantly affect the simulation of excess saturation. Although the vertical
439 discretization may affect the computed initial water content, this effect is usually negligible. It has
440 been found in other studies that the vertical discretization has little effect on simulated runoff due
441 to excess saturation [*Sulis et al.*, 2010].

442 **6.1.2 Excess infiltration**

443 When simulating excess infiltration the common node approach requires fully saturated conditions
444 at the topmost subsurface node for ponding to occur. However, top-down saturation associated
445 with excess infiltration implies that reaching fully saturated conditions in the topmost subsurface
446 discrete volumes should requires more time than reaching fully saturated conditions at the land
447 surface, especially if the vertical discretization is relatively coarse. It is thus expected that the
448 common node approach delays runoff and that this delay increases for a coarser vertical
449 discretization. In addition, if the saturation fronts are less sharp due to a relatively coarse vertical
450 discretization, it takes more time to reach saturated conditions at the common node. This will
451 further delay runoff. Indeed, the simulation results indicate clearly that runoff is delayed when
452 using the common node approach, particularly if the vertical discretization is relatively coarse
453 (Figure 6, 9a, 10 and 13a). It has also been found in other studies that the common node approach
454 delays runoff due to excess infiltration if the vertical discretization is relatively coarse [*Sulis et al.*,
455 2010].

456 As explained in Section 4.2, when using the consistent dual node approach, ponding due
457 to excess infiltration occurs before reaching fully saturated conditions at the topmost subsurface
458 node. More specifically, ponding occurs when the infiltrability is exceeded. Compared to the

459 condition for ponding in the common node approach this is arguably more correct. Namely, if
460 saturation occurs from the top-down then the saturation at a certain depth occurs later than
461 saturation at the land surface. Indeed, simulation results indicate that when simulating excess
462 infiltration the consistent dual node approach is less sensitive to the vertical discretization in
463 comparison to the common node approach. This is clearly indicated in Figure 6b-d, 9a, 10b-d and
464 13a. To further explain this difference in accuracy, it is emphasized that the spatial resolution only
465 affects the accuracy of the flow computations when using the consistent dual node approach and
466 that the formulation of head continuity at the interface remains correct. In contrast, when using the
467 common node approach, if the spatial resolution is too coarse then this does not only affect the
468 accuracy of the flow computations but in addition the formulation of head continuity becomes
469 incorrect. It must be emphasized, however, that regardless of the applied coupling approach, the
470 vertical discretization must be relatively fine. As indicated by Figure 6b-d, 9a, 10b-d and 13a the
471 difference between the simulated results and the reference solution increase for a coarser
472 discretization. Eventually such differences will lead to unreasonable results regardless of the
473 coupling approach.

474 It is interesting to note that An and Yu [*An and Yu*, 2014] also found that their model was
475 less sensitive to the vertical discretization in comparison to ParFlow when simulating runoff due
476 to excess infiltration. Whereas An and Yu [*An and Yu*, 2014] hypothesized that this difference in
477 performance was related to using irregular grids instead of orthogonal grids as in ParFlow, it is
478 argued here that this difference can be explained by the fact that both models use a different
479 coupling approach.

480 Although the consistent dual node approach is less sensitive to the vertical discretization
481 in comparison to the common node approach, it is useful to explain in detail how the vertical

discretization affects the accuracy of the consistent dual node approach to the vertical discretization. A relatively coarse vertical discretization may result in an underestimation of the vertical pressure gradient at the land surface. This is because in a soil close to hydrostatic conditions the pressure heads increase with depth. Therefore, the infiltrability during the early stages of infiltration may be underestimated. If the applied flux rate is sufficiently large such that the underestimated infiltrability is exceeded, then runoff during the early stages will be overestimated. Figure 6d illustrates that the runoff as simulated with the cell-centered scheme, a relatively coarse vertical discretization and a consistent dual node approach is indeed overestimated at early times. During the later stages of infiltration the pressure head at the topmost subsurface node will be underestimated due to the combined effect of an underestimated infiltration rate and the overly diffused saturation fronts. This results in an overestimation of the infiltration rate in the later stages. Thus at some time after ponding has started, it is expected that the amount of runoff is underestimated.

If the underestimated infiltrability is not exceeded, then the overly diffused saturation fronts resulting from a relatively coarse vertical discretization will eventually lead to an underestimation of pressure head at the topmost subsurface node and as such the infiltrability may be overestimated at later times. Consequently, when using the consistent dual node approach runoff due to excess infiltration may be delayed. However, the delay in runoff as simulated by the consistent dual node approach will only equal the delay in runoff as simulated by the common node approach in the limit when q_R/K_z goes to unity. Namely, as explained in Section 4.2 if q_R/K_z goes to unity, then the consistent dual node approach behaves similar as a common node approach. However, in general, if the consistent dual node approach delays runoff, this delay will be smaller than the delay in runoff as simulated by the common node approach.

Comparing Figure 12a and 13a it can be observed that if the vertical discretization is relatively coarse then a common node can act as an artificial barrier for a surface water wave advancing across an initially unsaturated subsurface domain. Namely, as the wave travels downstream the wave can only advance to the next common node once it is fully saturated. The effect of this artificial barrier is that the front of the surface water wave is steepened. In contrast, the consistent dual approach simulates a wave that becomes less steep as it advances downstream for relatively fine as well as relatively coarse vertical discretizations as depicted in Figure 13a.

As illustrated in Figure 6b-d, and 10b-d, if the coupling approach and the vertical discretization are identical, then the vertex-centered schemes are closer to the reference solution with respect to the cell-centered schemes. This difference results solely from the fact the primary mesh is the same for both schemes. As such the vertical extent of the topmost subsurface volumes is twice as small when using the vertex-centered scheme. This difference in vertical grid resolution near the land surface explains the differences between the schemes.

6.2 Computational efficiency

The computational efficiency of the schemes is measured in terms of the number of Newton steps. The number of Newton steps equals the number of times that the linearized system of equations is solved and this number depends on the time step sizes as well as the number of failed Newton steps. It is emphasized that the measured efficiency depends crucially on the applied model code. Nonetheless, as shown in the following, the measured differences in efficiencies can be explained in terms of abrupt changes in how fast pressure heads near the surface-subsurface interface are evolving with time. Regardless of the type of scheme used to solve the non-linear flow equations, such abrupt changes are difficult to solve.

Once ponding occurs a surface-subsurface flow model will encounter significant numerical difficulties as surface flow terms are activated. In essence, the activation of these terms represents a discontinuity in flow behaviour which is challenging to resolve [*Osei-Kuffuor et al.*, 2014]. Indeed, the Newton steps as depicted in Figure 3 and 7 indicate that simulations encounter difficulties at the moment of ponding. These figures also indicate that the consistent dual node approach can be more efficient in comparison to the common node approach.

6.2.1 Excess saturation

Just before the moment of ponding due to excess saturation, the rate of change in pressure heads at the topmost subsurface nodes is relatively high for both coupling approaches. This high rate is related to the shape of the water retention curve. Typically, the derivative of the saturation with respect to the pressure head goes to zero when approaching fully saturated conditions. Once ponding starts, the surface flow terms are activated and therefore the rate of changes in pressure heads at the topmost subsurface nodes decreases drastically. Both approaches must handle this drastic change. However, from Figure 4b and 5b it can be observed that the rate of change decreases more abruptly when using the common node approach.

When using the common node approach the vertical hydraulic gradients in the subsurface are close to zero at the moment of ponding, since additional water volumes can only be accommodated by means of specific storage. This implies that the infiltration rate drops instantaneously at the moment of ponding. In contrast, in the dual node approach ponding starts when the infiltrability is exceeded. Thus at the moment of ponding, the infiltration rate is higher in comparison to the common node approach. After ponding this infiltration rate will decrease quickly as the hydraulic heads at the dual nodes equilibrate. This difference in the infiltration rate at the moment of ponding explains why the topmost subsurface hydraulic heads change more

550 smoothly when using the dual node approach. If the vertical discretization is coarser, then the
551 infiltration rate at the moment of ponding as computed with the consistent dual node approach is
552 even higher and this results in a lower initial rate initial rate of change in water depth as depicted
553 in Figure 5a.

554 The more abrupt changes in pressure heads at the common node in comparison to the
555 changes in pressure heads at the dual nodes mean that solving the activation of ponding with the
556 common node approach is more difficult. It is noted that the differences in the infiltration rates
557 between the two coupling approaches only occur at the moment of ponding and directly thereafter
558 when water depths are relatively small. Namely, quickly after ponding, the hydraulic heads at the
559 dual nodes will equilibrate and after that the two coupling approaches will behave similar. This
560 explains why these differences in infiltration rates do not significantly affect the accuracy of
561 simulated runoff.

562 **6.2.2 Excess infiltration**

563 Figure 8, 9, 12 and 13 illustrate the evolution of pressure heads at dual nodes and common nodes
564 when simulating excess infiltration. When applying the consistent dual approach, the net flux into
565 a topmost subsurface cell will decrease once ponding occurs, because the applied flux rate will be
566 partitioned between dual nodes (i.e. between the surface flow and subsurface flow domain). This
567 occurs while the topmost subsurface node is not yet fully saturated. After ponding the infiltration
568 rate decreases such that if the topmost subsurface node reaches fully saturated conditions the net
569 flux into the topmost subsurface node is relatively small. In contrast, partitioning of the applied
570 flux rate on a common node between the surface flow and subsurface domain starts when the
571 common node reaches fully saturated conditions at this node. This means that just before ponding
572 the rate of change in pressure head is relatively high as the common node is driven towards fully

saturated conditions while the infiltration rate is relatively high. This means that similar to the excess saturation scenario the rate of change in pressure head at the common node is high just before ponding. At the moment of ponding, this rate must drop abruptly as surface flow terms are activated. This abrupt change explains why the common node approach is less efficient.

Figures 7 and 11 also indicate that a coarser vertical discretization only provides a significant gain in efficiency in terms of Newton steps when using the consistent dual node approach. When using the common node approach, a coarser discretization does not change the fact that the topmost subsurface node must reach fully saturated conditions for ponding to occur and that the infiltration rate is relatively high just before ponding. When using the consistent dual node approach, a coarser vertical discretization means that the saturation fronts are more diffused such that the flow problem becomes easier to solve.

Figure 8a and 9a illustrate that for the second simulation scenario, ponding occurs almost simultaneously at all the surface nodes. Figure 12a and 13a show that this is different for the third scenario where ponding occurs at different times as the flooding wave travels downstream. When Figure 11a is compared with Figure 12a and when Figure 11d is compared with Figure 13a, it is clear that the common node approach encounters difficulties around each time ponding starts at a surface node. Figure 11 shows that these difficulties are encountered for all discretizations. In contrast the consistent dual node approach has much less difficulties solving these difficulties. As discussed in Section 6.1.2. the common node approach may result in steepening the advancing wave. This implies that water depths will be changing more quickly. This presents an additional difficulty for solving this flow problem with the common node approach.

7 Conclusions

In this study it is shown that the dual node approach should be conceptualized and implemented as a one-sided finite differences approximation of the vertical hydraulic gradient at the land surface. This provides an important new insight into the coupling length. Namely, if the dual node approach is properly implemented then the coupling length is related to the vertical grid resolution. Thus, the coupling length does not represent an additional non-physical model parameter and therefore the dual node approach is not automatically a less physically based approach in comparison to the common node approach. Actually, this study shows if the vertical discretization is not sufficiently fine then the head continuity at the surface-subsurface interface is formulated more correctly in the consistent dual node scheme. This difference in formulation has consequences for how both approaches compare in terms of accuracy and efficiency.

Numerical experiment indicate that the consistent dual node approach is equally accurate or more accurate than the common node approach. It has been shown that in comparison to the common node approach the consistent dual node approach is less sensitive to the vertical discretization when simulating excess infiltration. However, the practical advantage of the consistent dual node approach in terms of accuracy is limited. Namely, if the vertical discretization is refined, both approaches will converge to more accurate and eventually similar results when simulating excess infiltration. When simulating excess saturation both approaches yield similar results even if the vertical discretization is relatively coarse.

Nonetheless, even though the advantage of the consistent dual node approach in terms of accuracy is limited, the fact that the consistent dual node approach is equally or more accurate than the common node approach is a significant finding. Namely, this finding is different from the commonly held view that a dual node approach is most accurate if it mimics the common node

617 approach. Moreover, it also illustrates clearly that the consistent dual node approach is not similar
618 to a common node approach.

619 Numerical experiment indicate that the consistent dual node approach can be more efficient
620 than the common node approach while being equally or more accurate than the common node
621 approach. It has been shown that this difference in efficiency is related to abrupt changes in the
622 evolution of pressure heads around the moment that ponding is initiated.

623 Based on the findings in this study the models of An and Yu [*An and Yu*, 2014] and Kumar
624 et al. [*Kumar et al.*, 2009] are expected to have some advantages with respect to models that are
625 based on the common node approach. This is because these models are based on a consistent dual
626 node approach. Moreover, given a model that uses an alternative dual node approach, it is relatively
627 straightforward to implement the numerically more correct consistent dual node approach.

628

629 **Acknowledgements**

630 This research was funded by the Carl. S. Swisher Foundation.

631

632 **References**

633 An, H., and S. Yu (2014), Finite volume integrated surface- subsurface flow modeling on
634 nonorthogonal grids, *Water Resources Research*, *50*(3), 2312-2328.
635 Blazek, J. (2005), *Computational fluid dynamics: Principles and applicationsComputational fluid*
636 *dynamics: Principles and applications*, Elsevier.
637 Camporese, M., C. Paniconi, M. Putti, and S. Orlandini (2010), Surface-subsurface flow modeling
638 with path-based runoff routing, boundary condition-based coupling, and assimilation of
639 multisource observation data, *Water Resources Research*, *46*.
640 De Rooij, R., W. Graham, and R. Maxwell (2012), A particle-tracking scheme for simulating
641 pathlines in coupled surface-subsurface flows, *Advances in Water Resources*.

de Rooij, R., P. Perrochet, and W. Graham (2013), From rainfall to spring discharge: Coupling conduit flow, subsurface matrix flow and surface flow in karst systems using a discrete-continuum model, *Advances in Water Resources*, *61*, 29-41.
Delfs, J. O., C. H. Park, and O. Kolditz (2009), A sensitivity analysis of Hortonian flow, *Advances in Water Resources*, *32*(9), 1386-1395.
Diersch, H. J. G., and P. Perrochet (1999), On the primary variable switching technique for simulating unsaturated-saturated flows, *Advances in Water Resources*, *23*(3), 271-301.
Ebel, B. A., B. B. Mirus, C. S. Heppner, J. E. VanderKwaak, and K. Loague (2009), First-order exchange coefficient coupling for simulating surface water-groundwater interactions: parameter sensitivity and consistency with a physics-based approach, *Hydrological Processes*, *23*(13), 1949-1959.
Gaukroger, A. M., and A. D. Werner (2011), On the Panday and Huyakorn surface-subsurface hydrology test case: analysis of internal flow dynamics, *Hydrological Processes*, *25*(13), 2085-2093.
Hillel, D. (1982), *Introduction to soil physics*, Academic press New York.
Kolditz, O., and H. Shao (2010), OpenGeoSys, Developer-Benchmark-Book, OGS-DBB 5.04, Helmholtz Centre for Environmental Research (UFZ).
Kollet, S. J., and R. M. Maxwell (2006), Integrated surface-groundwater flow modeling: A free-surface overland flow boundary condition in a parallel groundwater flow model, *Advances in Water Resources*, *29*(7), 945-958.
Kumar, M., C. J. Duffy, and K. M. Salvage (2009), A Second-Order Accurate, Finite Volume-Based, Integrated Hydrologic Modeling (FIHM) Framework for Simulation of Surface and Subsurface Flow, *Vadose Zone Journal*, *8*(4), 873-890.
Liggett, J. E., A. D. Werner, and C. T. Simmons (2012), Influence of the first-order exchange coefficient on simulation of coupled surface-subsurface flow, *Journal of Hydrology*, *414*, 503-515.
Liggett, J. E., M. J. Knowling, A. D. Werner, and C. T. Simmons (2013), On the implementation of the surface conductance approach using a block-centred surface-subsurface hydrology model, *Journal of Hydrology*, *496*, 1-8.
Morita, M., and B. C. Yen (2002), Modeling of conjunctive two-dimensional surface-three-dimensional subsurface flows, *Journal of Hydraulic Engineering-Asce*, *128*(2), 184-200.
Moukalled, F., L. Mangani, and M. Darwish (2016), *The Finite Volume Method in Computational Fluid Dynamics*, Springer.
Osei-Kuffuor, D., R. M. Maxwell, and C. S. Woodward (2014), Improved numerical solvers for implicit coupling of subsurface and overland flow, *Advances in Water Resources*, *74*, 185-195.
Pan, L., and P. J. Wierenga (1995), A transferred pressure head based approach to solve Richards equation for variably saturated soils, *Water Resources Research*, *31*(4), 925-931.
Panday, S., and P. S. Huyakorn (2004), A fully coupled physically-based spatially-distributed model for evaluating surface/subsurface flow, *Advances in Water Resources*, *27*(4), 361-382.
Ross, P. J. (1990), Efficient numerical methods for infiltration using Richards equation, *Water Resources Research*, *26*(2), 279-290.
Sulis, M., S. B. Meyerhoff, C. Paniconi, R. M. Maxwell, M. Putti, and S. J. Kollet (2010), A comparison of two physics-based numerical models for simulating surface water-groundwater interactions, *Advances in Water Resources*, *33*(4), 456-467.
Therrien, R., R. G. McLaren, E. A. Sudicky, and S. M. Panday (2010), HydroGeoSphere-a three-dimensional numerical model describing fully-integrated subsurface and surface flow and solute transport (draft), Groundwater Simulations Group, University of Waterloo.

VanderKwaak, J. E. (1999), Numerical simulation of flow and chemical transport in integrated surface-subsurface hydrologic systems, University of Waterloo.
Yeh, G.-T., D.-S. Shih, and J.-R. C. Cheng (2011), An integrated media, integrated processes watershed model, *Computers & Fluids*, *45*(1), 2-13.
Zienkiewicz, O., R. Taylor, and J. Zhu (2005), The finite element method: its basis and fundamentals. 2005, edited, Butterworth-Heinemann.

abbreviation	meaning
cc	cell-centered
vc	vertex-centered
dn	dual node
cn	common node

Table 1: Abbreviations as used in the figures.

a)

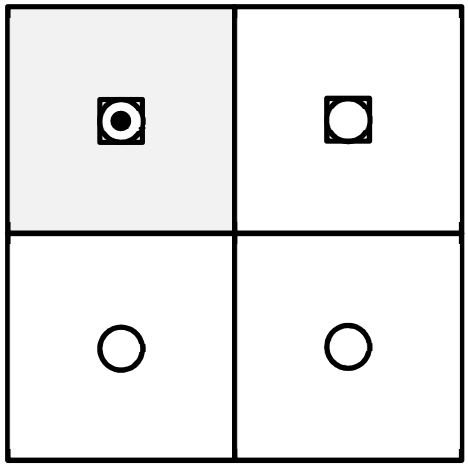

b)

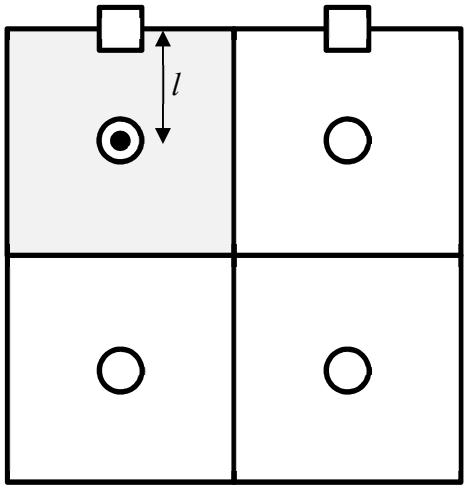

c)

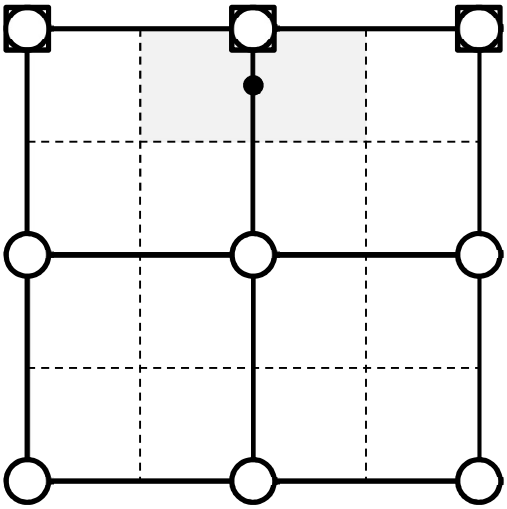

d)

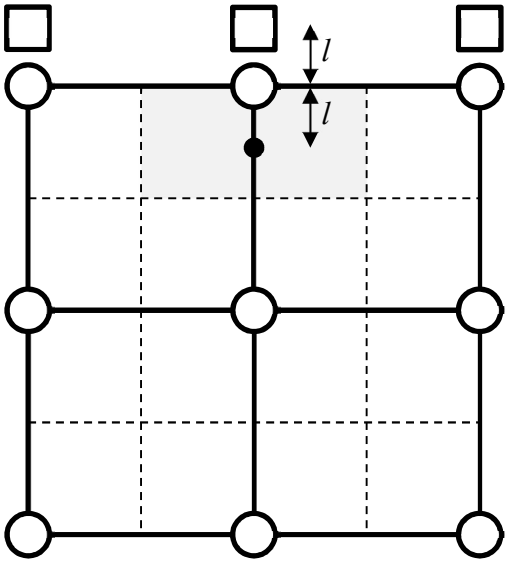

Figure 1: a) Common nodes in cell-centered schemes. b) Dual nodes in cell-centered-centered schemes. c) Common nodes and co-located dual nodes in vertex-centered schemes. d) Dual nodes in vertex-centered schemes (not co-located). The white squares and white circles represent surface and subsurface nodes, respectively. The solid and dashed lines represent the primary mesh and the dual mesh, respectively. The grey-shaded area is a topmost discrete volume as associated with a topmost subsurface node. The black dot represents the centroid of this volume. The coupling length l as depicted in this figure applies to the consistent dual node approach.

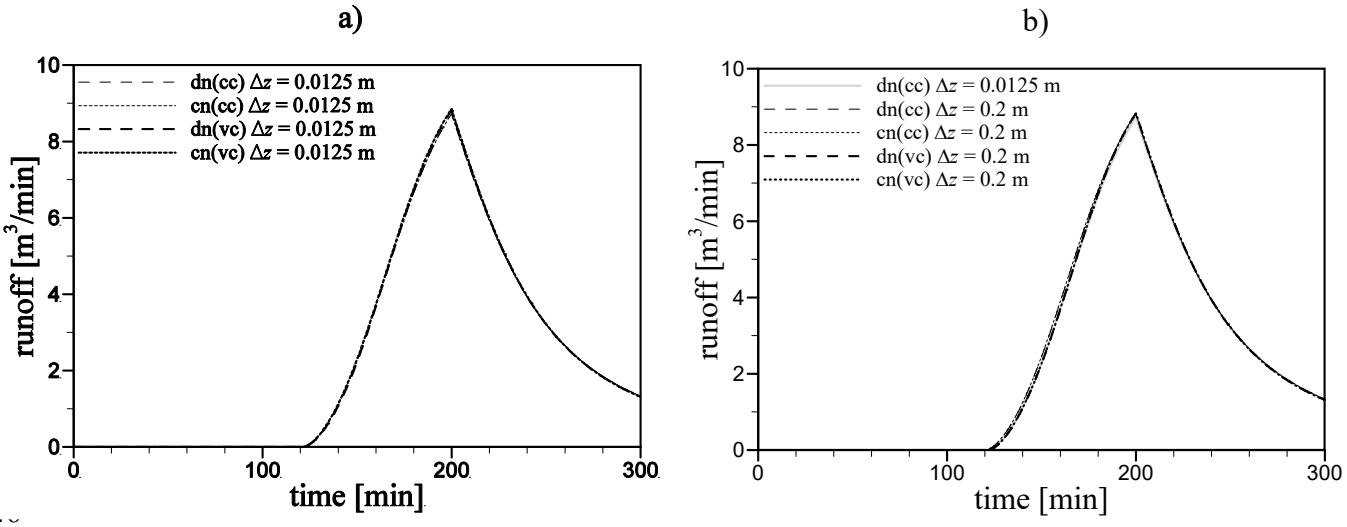

Figure 2: Outflow response for excess saturation on a hillslope (first scenario) using different vertical discretizations.

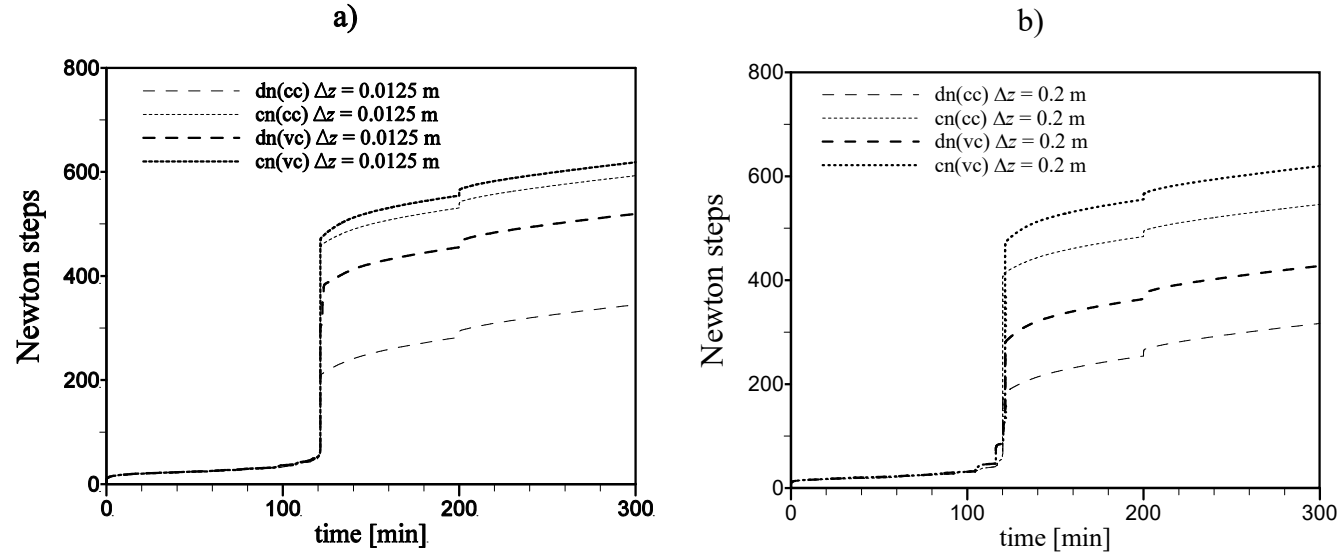

Figure 3: Number of Newton steps for excess saturation on a hillslope (first scenario) using different vertical discretizations.

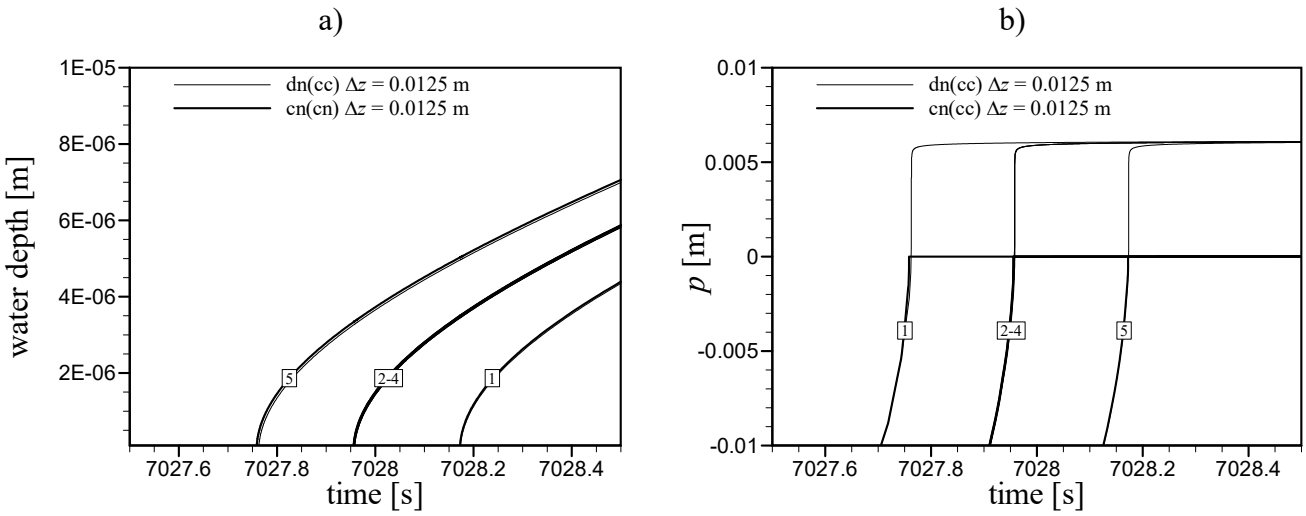

Figure 4: Simulated values at the common nodes for excess saturation on a hillslope (first scenario) with a cell-centered scheme and Δz = 0.0125 m. a) Water depths. b) Pressure heads. Nodes are numbered 1-5 in the down-slope direction.

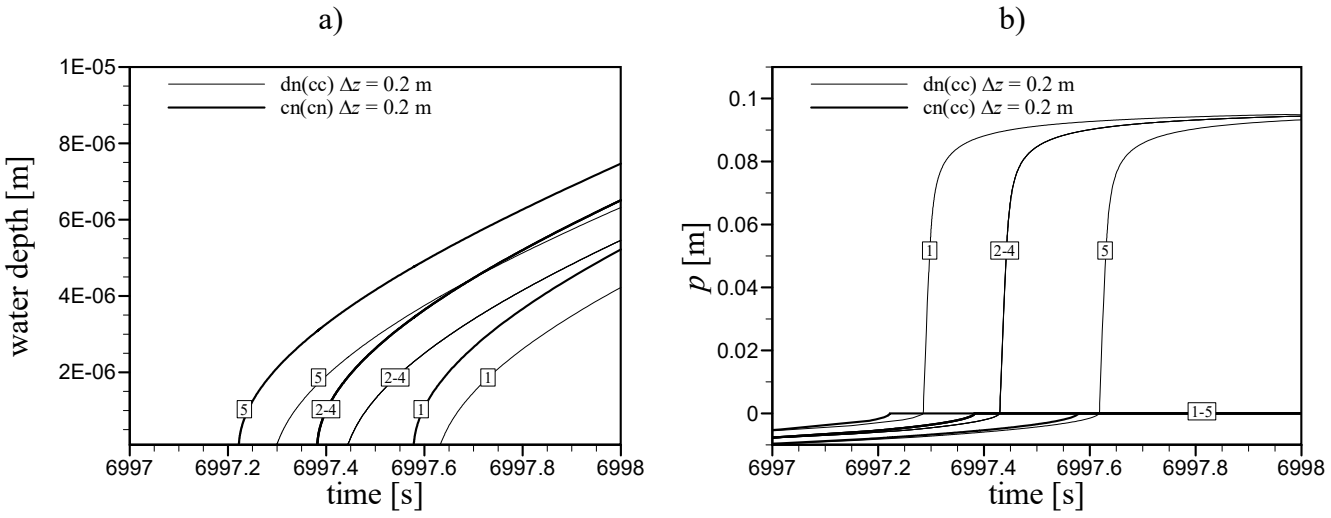

Figure 5: Simulated values for excess saturation on a hillslope (first scenario) with a cell-centered scheme and Δz = 0.2 m. a) Water depths at the surface nodes. b) Pressure heads at the topmost subsurface nodes. Nodes are numbered 1-5 in the down-slope direction.

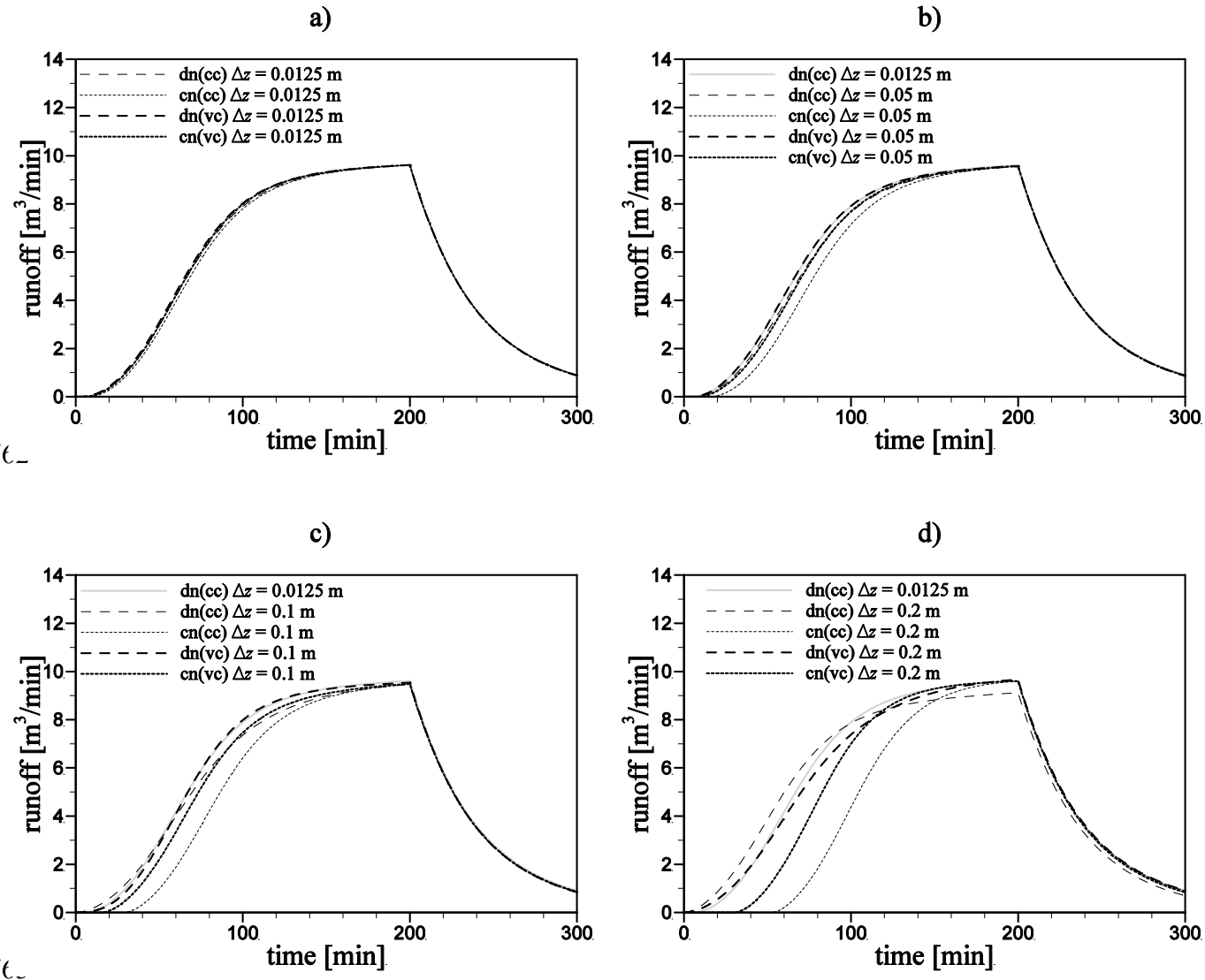

Figure 6: Outflow response for excess infiltration on a hillslope (second scenario) using different vertical discretizations.

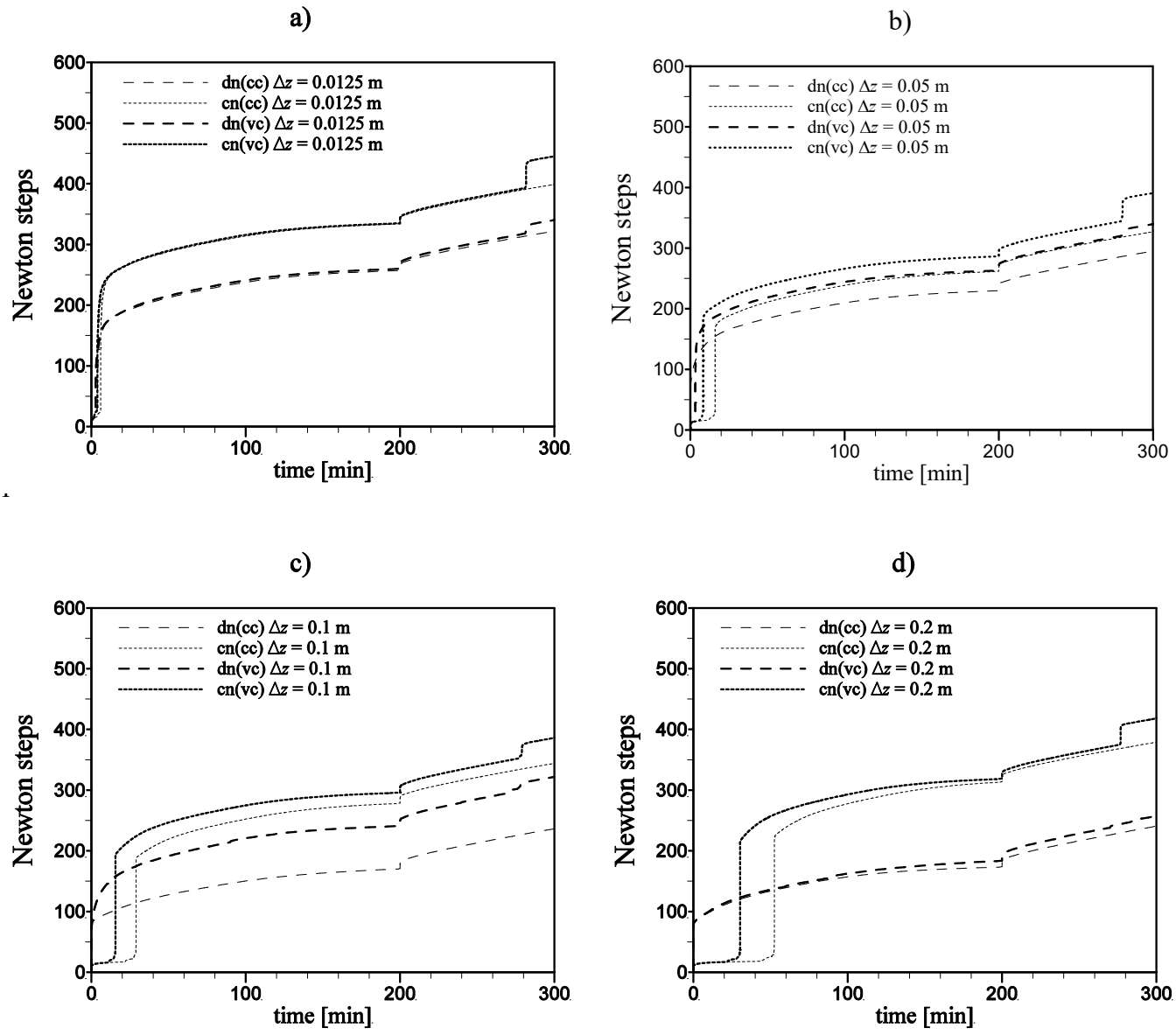

Figure 7: The total number of Newton steps for excess infiltration (second scenario) on a hillslope using different vertical discretizations.

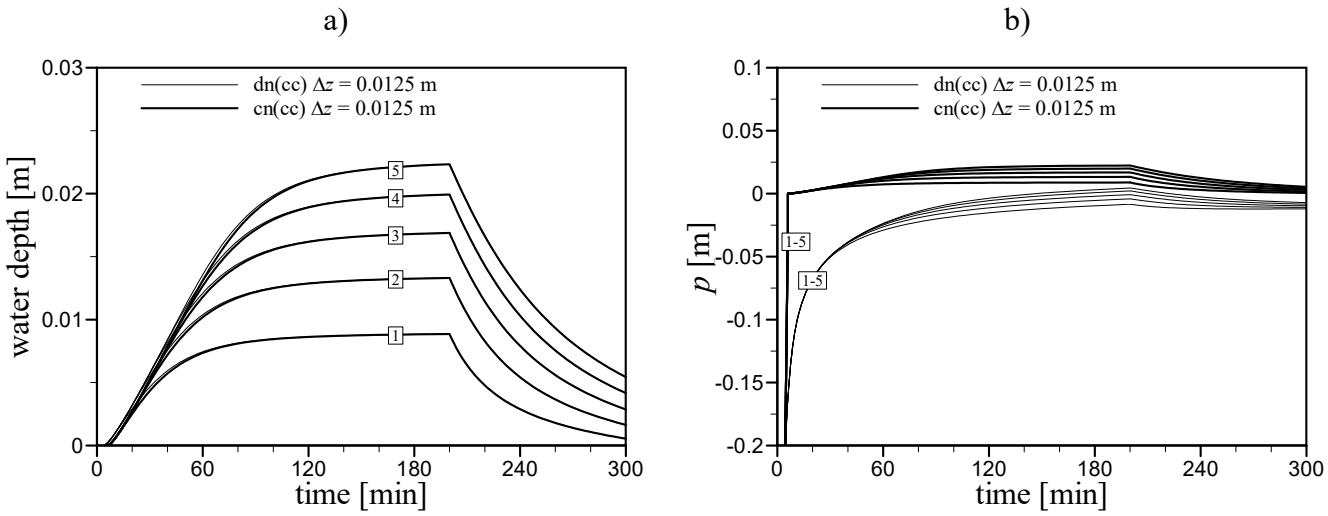

Figure 8: Simulated values at the common nodes for excess infiltration on a hillslope (second scenario) with a cell-centered scheme and Δz = 0.0125 m. a) Water depths. b) Pressure heads. Nodes are numbered 1-5 in the down-slope direction.

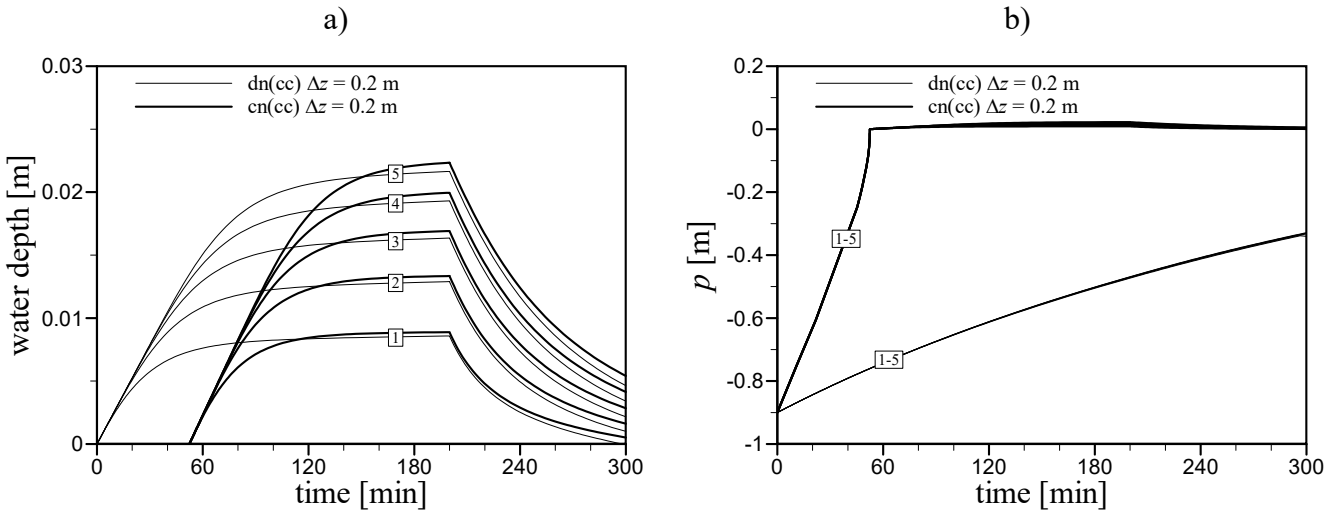

Figure 9: Simulated values for excess infiltration on a hillslope with a cell-centered scheme (second scenario) and Δz = 0.2 m. a) Water depths at the surface nodes. b) Pressure heads at the topmost subsurface nodes. Nodes are numbered 1-5 in the down-slope direction.

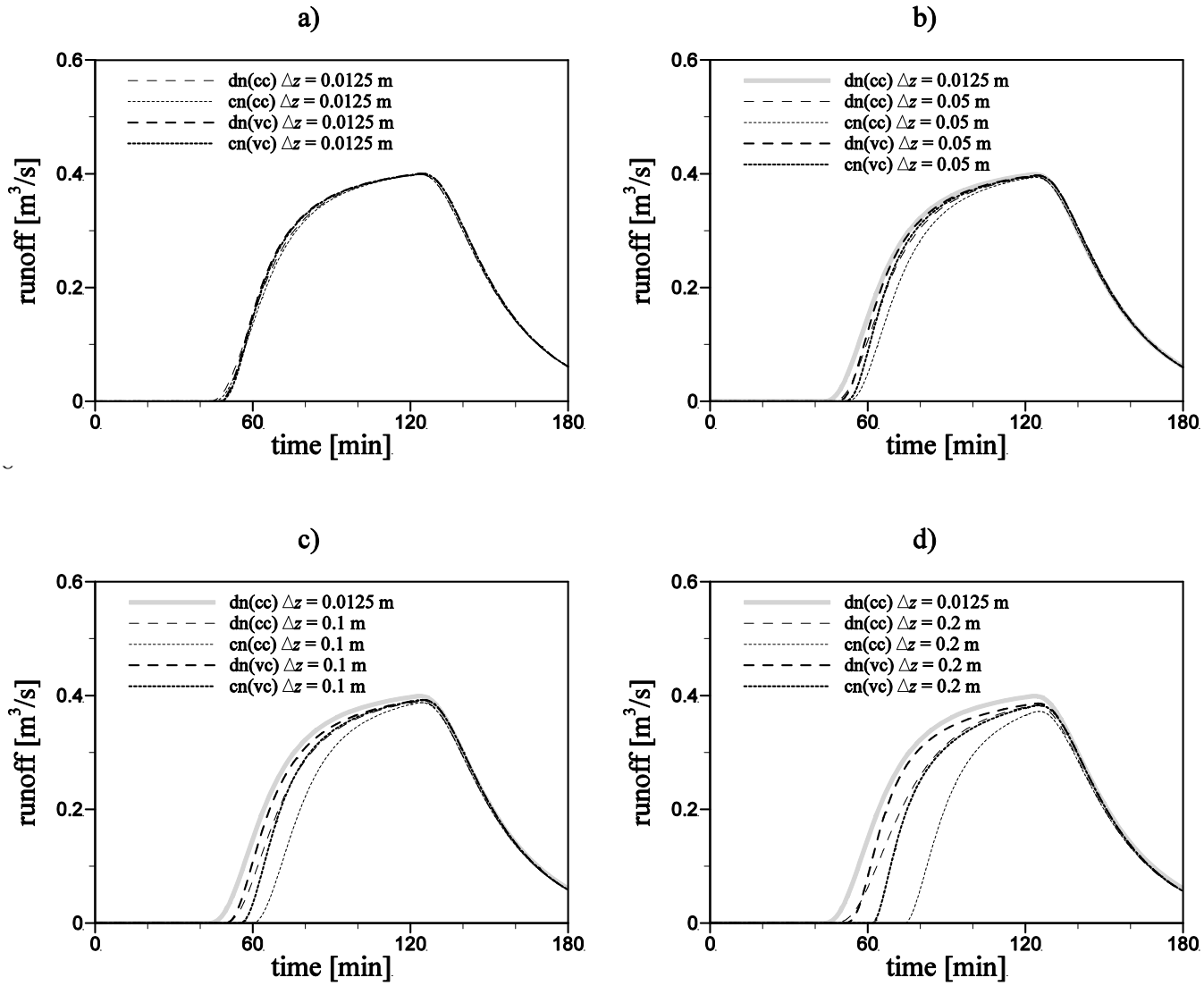

Figure 10: Outflow response for flooding an unsaturated hillslope using different vertical discretizations.

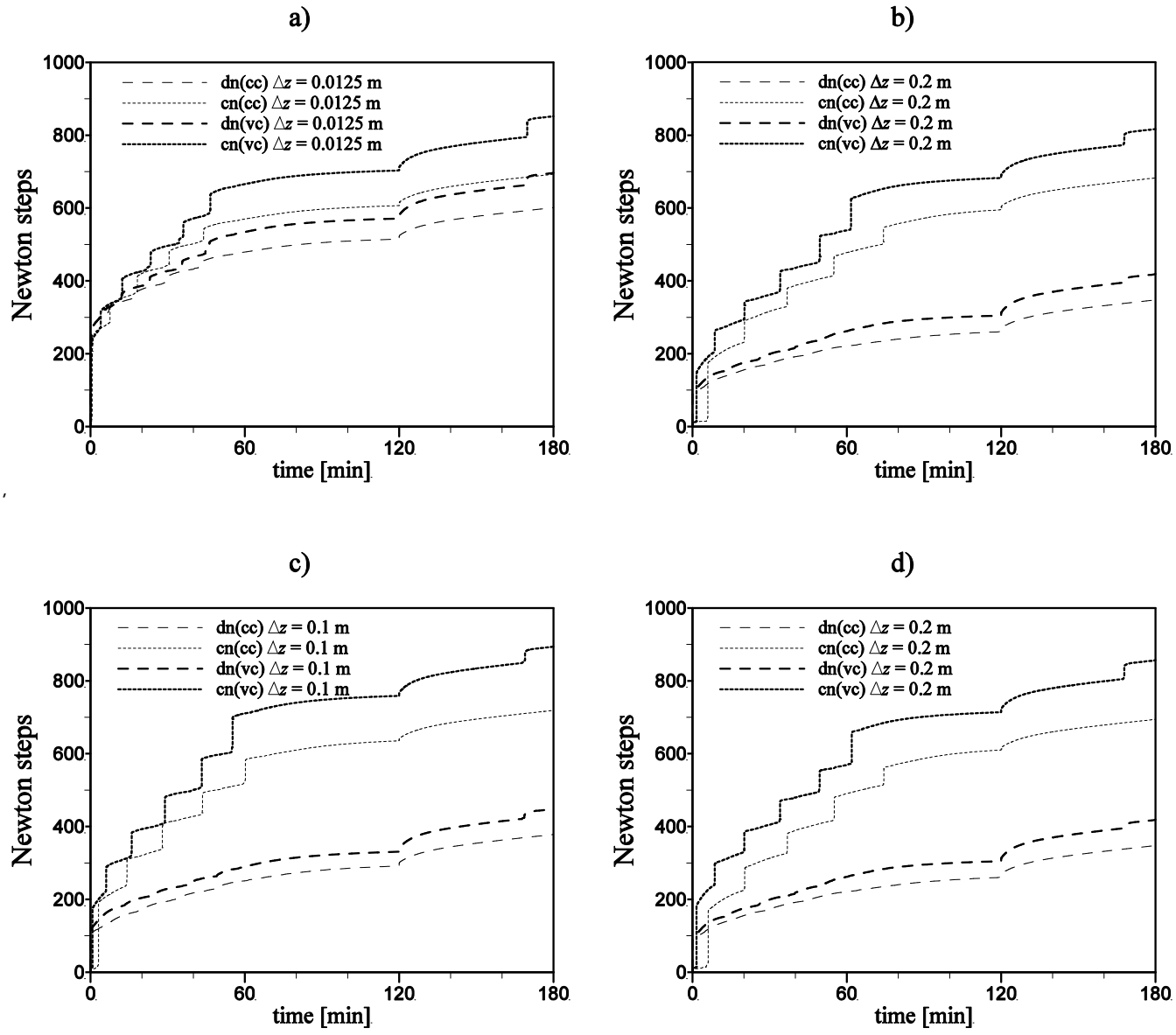

Figure 11: Number of Newton steps for flooding an unsaturated hillslope using different vertical discretizations.

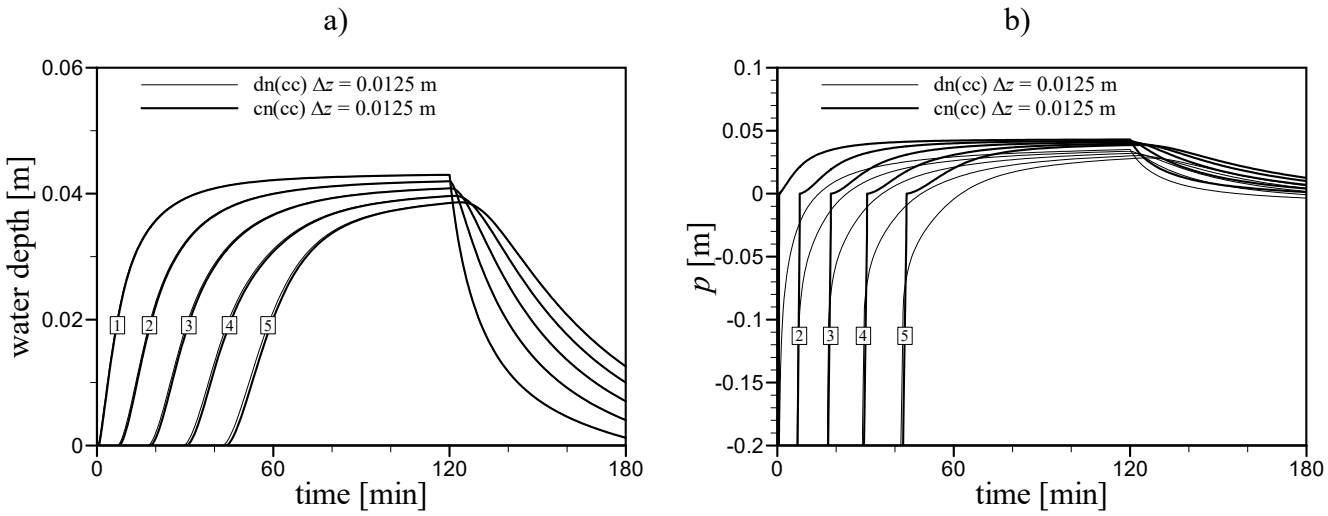

Figure 12: Simulated values for excess infiltration (third scenario) on a hillslope with a cell-centered scheme and $\Delta z = 0.0125$ m. a) Water depths at the surface nodes. b) Pressure heads at the topmost subsurface nodes. Nodes are numbered 1-5 in the down-slope direction).

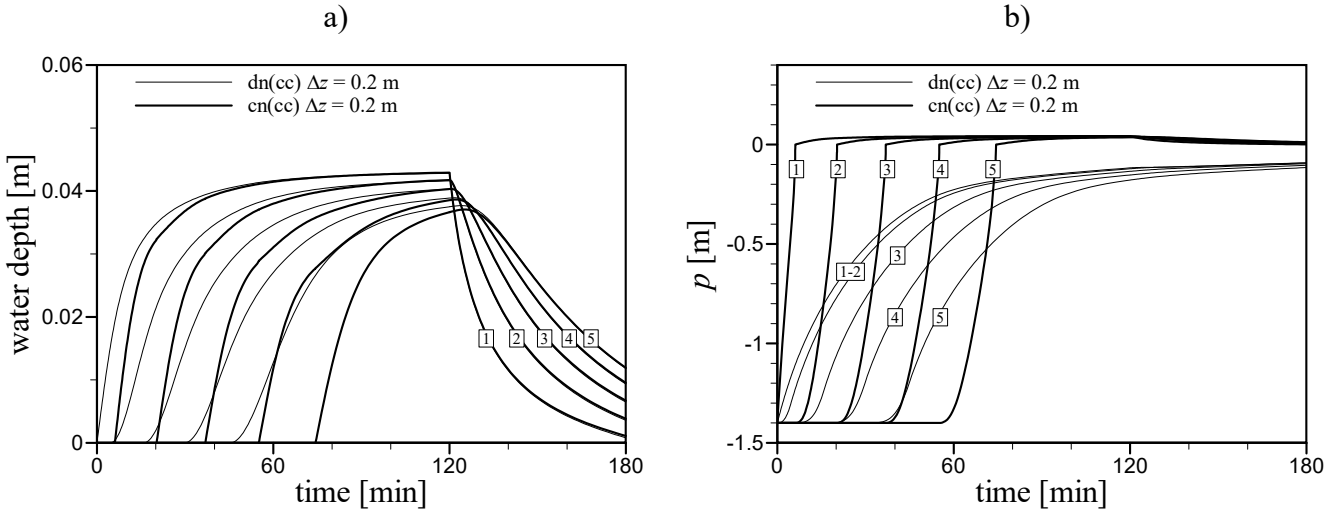

Figure 13: Simulated values for excess infiltration (third scenario) on a hillslope with a cell-centered scheme and $\Delta z = 0.2$ m. a) Water depths at the surface nodes. b) Pressure heads at the topmost subsurface nodes. Nodes are numbered 1-5 in the down-slope direction).